

# ON THE STRUCTURE AND DYNAMICAL FEATURES OF INTERLEAVING IN THE ARCTIC OCEAN

Natalia Kuzmina<sup>1</sup>, Bert Rudels<sup>2,3</sup>, Victor Zhurbas<sup>1</sup>, Tapani Stipa<sup>2</sup> and Natalia Zhurbas<sup>4</sup>

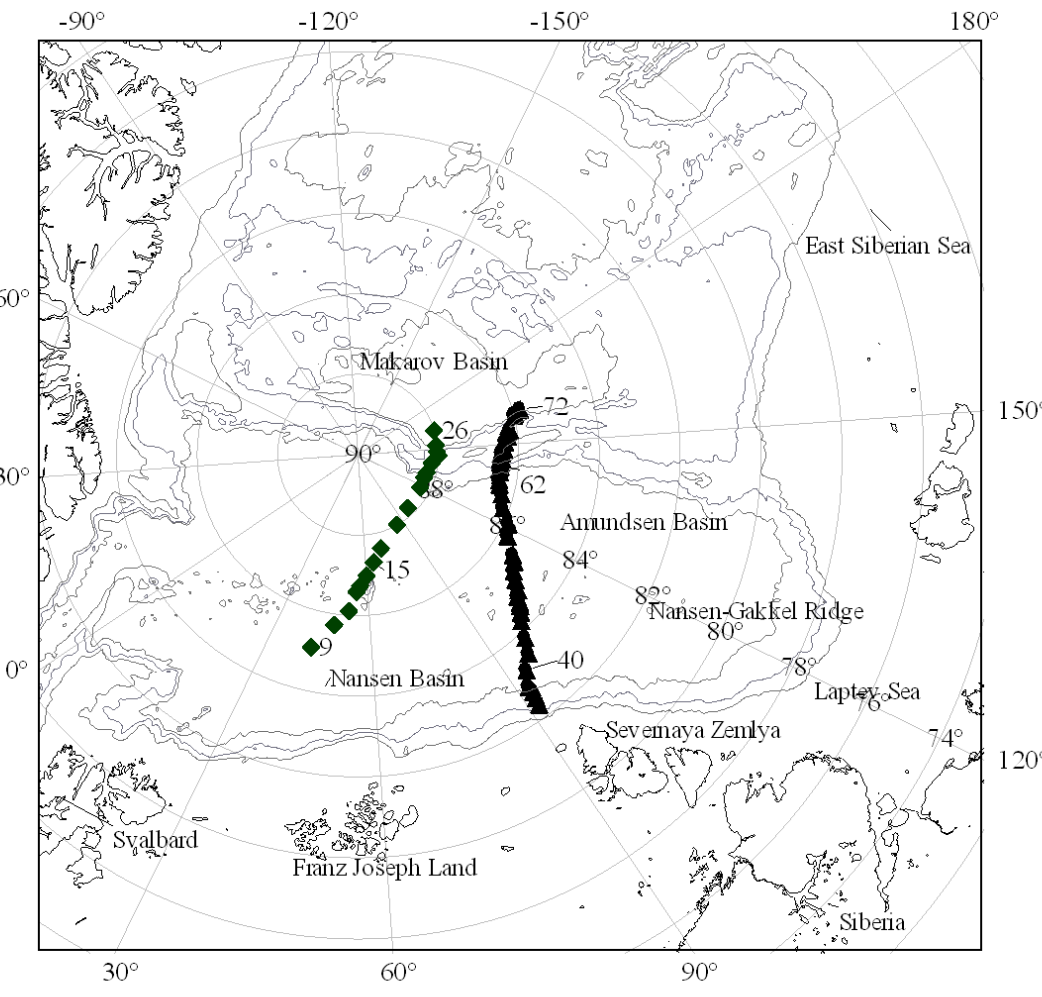
<sup>1</sup>Shirshov Institute of Oceanology, Moscow, Russia

<sup>2</sup>Finnish Meteorological Institute, Helsinki, Finland

<sup>3</sup>Department of Physics, University of Helsinki, Finland

<sup>4</sup>Moscow Physical and Technical Institute

EGU



## Introduction

Here we shall model the interleaving structures observed in the Arctic Ocean. The focus will be on evaluating coefficients of diffusivity and comparing the estimates with results obtained by Walsh and Carmack [2002, 2003]. We shall also theoretically analyse the slopes of unstable modes due to combined effect of baroclinicity and differential mixing at fronts found in the stable-stable stratification.

However, before this is attempted a detailed and quantified description and classification of the different intrusive layer structures encountered in the Arctic Ocean will be given. The focus of our investigation is to study not only structures of interleaving but also structure of the fronts where the interleaving was observed. This was not done earlier.

## Data

The CTD observations used were obtained in the Nansen, Amundsen basins and over the Lomonosov Ridge from R/V *Polarstern* in 1996 (hereafter PS-96), IB *Oden* in 1991 (Oden-91) (Fig. 1). The instruments used were Neil Brown MarkIIIb CTDs and occasionally Sea-bird SBE-11. Fig. 1 gives positions of all CTD casts used in the analysis. Detailed descriptions of the data are given, for example, in Carmack et al. [1997], Rudels et al. [1999].

## Empirical analysis of structural features of intrusive layers

Fig. 2 shows a sequence of salinity profiles from the main PS-96 transect. Here three different types of large intrusive layers can be distinguished, depending upon the length scales and the shapes of salinity and temperature profiles and the mean thermohaline stratification:

- (1) Inversions and intrusive layers in the upper part of the thermocline where the stratification is favorable for diffusive convection;
- (2) Large, extensive inversions and intrusive layers present between the temperature maximum and the salinity maximum but extending below the salinity maximum. The stratification is here either absolutely stable (upper part) or unstable in the salting sense (lower part);
- (3) Deep intrusive layers existing at absolutely stable thermohaline stratification;

## Upper layer intrusions (type 1)

The most intensive intrusions are observed at stations 37-39 between 150m and 220m (Fig.3). The vertical scale of intrusions is approximately 30-40 meters. The corresponding vertical profiles in temperature and salinity can in some cases be referred to as having a "saw-tooth" or "cog" structure (st.37-39), where relatively thin high gradient layers of the increasing temperature and salinity with depth are interleaved with thicker, low gradient layers of decreasing temperature and salinity with depth. The T, S and - diagrams in Fig. 4 show that warm and salty (cold and fresh) intrusions crossing the front become heavier (lighter) in accordance with a dominating buoyancy transport through the diffusive interfaces. Fig.4b demonstrates that T, S-characteristics of the salting stratification layers are grouped in well defined lines crossing the isopycnals.

## Large-scale intrusive layers in the vicinity of the salinity maximum (type 2)

The large-scale intrusive layers observed in the depth range of 200-600 m are characterized by high coherence over distances of the same order as the Eurasian Basin (Fig. 2). The intrusions in temperature and salinity display a well-pronounced "saw-tooth" or "cog" appearance. The thickness of the high-gradient layers is 20-30 m, while the low-gradient layers are much thicker (100 m and more).

The profiles on stations 42 and 54 are substantially different from those on the adjacent stations. This can be understood by examining salinity and temperature sections drawn using data from stations 30 to 72 (Fig. 6). Here stations 42 and 54 can be identified by the presence of isolated boluses of saline and warmer water, which may be interpreted as meso-scale, anticyclonic eddies [Schauer et al., 2002]. This would then indicate that meso-scale eddies can move as isolated water bodies through the layer structures without losing their identity.

Fig. 7 shows T, S curves from stations 40,41,43-56. The T, S curves from stations 40,41,43-46 indicate that warm and saline (cold and fresh) intrusions descend (rise) relative to the isopycnal surfaces. At the stations 47-56 T, S-curves show practically an alignment of the layers with the isopycnals. It is worthwhile to stress that T, S-characteristics of the salting stratification layers are grouped in well defined lines only where layers intersect the isopycnals (stations 41, 43-46).

## Deep intrusive layers at stable-stable thermohaline stratification (type 3)

Fig. 9 shows vertical profiles (left side of the figure) of density (top), temperature (centre), and salinity (bottom) from stations 36-50 for the depth range of 600 -1050 m. Deeper, between 800 and 1050 m, in the region of absolutely stable thermohaline stratification, intensive, coherent intrusive layers are observed having clearly expressed "saw-tooth" shape in the salinity and temperature profiles. The thickness of high-gradient layers, where temperature and salinity increase with depth, is 10 m, while the low-gradient layers, with temperature and salinity decreasing with depth, are about three times as thick (30-40 m).

T, S-diagram drawn for stations 36-50 and the depth range of 800-1050 m (Fig. 10) reveals the presence of two water masses, one warm and saline, the other cold and fresh. Between the T, S-curves of the "parent" water masses the T, S-curves display high variability due to the presence of intrusive layers. The intrusive layers are coherent, and cross the isopycnals with warm and saline (cold and fresh) intrusions becoming more (less) dense. This fact, together with information about the slopes of isopycnal surfaces to the horizontal (Fig. 9), shows that the intrusions slope more strongly than the isopycnals. Thus, the slope of the intrusions lies outside the wedge of baroclinic instability [May and Kelley, 1997; Kuzmina and Zhurbas, 2000], where potential energy of mean density field can be transformed into kinetic energy of the disturbances.

## 2. Model Setup

We apply the Princeton Ocean Model – POM (Blumberg and Mellor 1983). The POM is primitive equation,  $\sigma$  coordinate, free surface, hydrostatic model with 2.5 moment turbulence closure sub-model (Mellor and Yamada 1982) embedded. The model domain includes the whole Baltic Sea closed at the straits; the digital topography is taken from (Seifert et al. 2001). A model grid with varying grid spacing refined to 0.5 nm in the Gulf is applied; there are 20  $\sigma$  layers in the vertical direction. The atmospheric forcing (wind stress and heat flux components) for a 20-day period starting on 20 July 1999 was taken from a meteorological data set established and maintained by Lars Meuller at the Swedish Meteorological and Hydrological Institute (SMHI). The wind stress field calculated from the SMHI data set was eventually calibrated to fit the wind observations at Kalbadagrund weather station (Finnish Meteorological Institute). The initial thermohaline fields were constructed with the help of Data Assimilation System coupled with the Baltic Environmental Database established and maintained by Alexander Sokolov and Fredrik Wulff at the Stockholm University (see <http://data.ecology.su.se/models>). The model runs were started from the motionless state.

## 4. Lateral eddy diffusivity estimates

The numerical simulation data are used to estimate the apparent lateral diffusivity produced by the squirts. To arrive to the direct lateral diffusivity estimates, the fluctuations of temperature and transversal component of the flow velocity in the surface layer were extracted at 3 along-gulf transects (see Fig.2b) by means of high-pass filtering of the simulated data with the averaging length of the range of 40-90 km, and their cross-correlation was divided by the mean transverse temperature gradient:

$$K_{eddy} = \langle V'T' \rangle / \langle \partial T / \partial y \rangle$$

The time dependence of the lateral diffusivity,  $K_{eddy}$ , is shown in Figure 3. During the first five days of the upwelling period (July 21-25) estimates of lateral eddy diffusivity are negligible varying around zero within a range of  $30 \text{ m}^2 \text{ s}^{-1}$ , which corresponds to a relatively stable development of longshore baroclinic upwelling/downwelling jets. Then, displays a sudden increase to approximately  $500 \text{ m}^2 \text{ s}^{-1}$  within a couple of days. This corresponds to swelling of instability of the longshore baroclinic jets in the form of cold and warm squirts/filaments which eventually can be transformed to mushroom structures and eddies. The value of remains high even after the westerly winds cease, i.e. during the relaxation period of coupled upwelling/downwelling. Therefore, instability of longshore baroclinic jets may be considered as the major process contributing to relaxation of upwelling/downwelling.

## 5. Conclusions

- 1) Mesoscale coherent structures (filaments or squirts) and the whole process of relaxation of temperature field observed in the Gulf after upwelling event were reasonably well reproduced by the model;
- 2) Numerical simulations showed that the relaxation of longshore baroclinic jets and related thermohaline fronts caused by coupled upwelling and downwelling events in the Gulf occurs in the form of cold and warm water squirts running back and forth across the Gulf and thereby contributing to lateral mixing. Using simulated pseudo-random fields of temperature and current velocity, the lateral eddy diffusivity in the surface layer due to squirts was directly estimated at  $5 \cdot 10^2 \text{ m}^2 \text{ s}^{-1}$ .

## References

- Blumberg, A. F., and G. L. Mellor, Diagnostic and prognostic numerical calculation studies of the South Atlantic Bight, *J. Geophys. Res.*, 88, pp. 4579-4592, 1983.
- Mellor, G. L., and T. Yamada, Development of a turbulence closure model for geophysical fluid problems, *Rev. Geophys.*, 20, pp. 851-875, 1982
- Seifert, T., F. Tauber and B. Kayser, A high resolution spherical grid topography of the Baltic Sea – revised edition. Baltic Sea Science Congress 2001: Past, Present and Future – A Joint Venture. Abstract Volume. Stockholm Marine Research Centre, Stockholm University, p. 298, 2001. Web reference: [http://www.iowarnemuende.de/en\\_lowtopo.html](http://www.iowarnemuende.de/en_lowtopo.html).
- Vahtera E., J. Laanemets, J. Pavelson, M. Huttonen, K. Kononen, Effect of upwelling on the pelagic environment and bloom-forming cyanobacteria in the western Gulf of Finland, Baltic Sea, *J. Mar. Sys.*, 58, pp. 67-82, 2005.
- Zhurbas, V., I. S. Oh, and T. Park, Formation and decay of a longshore baroclinic jet associated with transient coastal upwelling and downwelling: A numerical study with applications to the Baltic Sea, *J. Geophys. Res.*, 111, C04014, doi:10.1029/2005JC003079, 2006.

